



North-South Differences of Xuefeng Mountain Metallogenic Belt and Fluid Inclusion and Isotope Evidences of Ore-Forming Hydrothermal Solution Source

Xingyu Ding¹, Liangliang Jia^{2,3*}

¹ School of Civil Engineering, Hunan City University, Yiyang 413000, China

² College of Engineering, Zunyi Normal University, Zunyi 563006, China

³ MOE Key Laboratory of Metallogenic Prediction of Nonferrous Metals, School of Geosciences and Info-Physics, Central South University, Changsha 410083, China

Corresponding Author Email: jialiangliang1986@zync.edu.cn

<https://doi.org/10.18280/ijht.410306>

ABSTRACT

Received: 25 February 2023

Accepted: 26 April 2023

Keywords:

Xuefeng Mountain metallogenic belt, ore-forming differences, fluid inclusions, ore-forming hydrothermal solution

Single gold deposits are mainly found in the southern section of the Xuefeng Mountain metallogenic belt, and gold-antimony-tungsten polymetallic deposits are gradually found northward. Based on the causes of ore-forming differences between the southern and northern sections, this research studied fluid inclusion characteristics and hydrogen and oxygen isotopes of the main gold-bearing mineral quartz in both sections. The test results show that the cationic composition of quartz fluid inclusions in typical gold deposits in the southern section is Na⁺-Ca²⁺ type, and the anionic composition is mainly SO₄²⁻ and Cl⁻, with K⁺/Na⁺<1 and F⁻/Cl⁻<1. The CO₂ and N₂ content in the gas phase composition is extremely low, especially with the maximum N₂ content of only 0.025μg·g⁻¹. Hydrogen and oxygen isotope projection falls near the formation and metamorphic water, indicating that the ore-forming fluids do not come from magmatic water. The cationic content of quartz fluid inclusions in typical gold deposits in the northern section is relatively dispersed, including Ca⁺ enriched type and Na⁺-K⁺-Ca²⁺ type, and the anionic composition is mainly SO₄²⁻. The CO₂ and N₂ content indicating deep source in the gas phase composition is much higher than that of gold deposits in the southern section, and pure N₂ inclusions are developed. Hydrogen and oxygen isotope projection mainly falls into the formation and metamorphic water and their overlap area. The geological and geochemical characteristics show that the ore-forming hydrothermal solution in the southern section mainly comes from groundwater, and that in the northern section comes from a mixture of magmatic rocks, metamorphic water, and groundwater.

1. INTRODUCTION

As one of the most important gold-polymetallic metallogenic belts in South China, the Xuefeng Mountain arc-shaped gold-polymetallic metallogenic belt (hereinafter referred to as the "Xuefeng Mountain metallogenic belt") is mainly rich in gold, followed by antimony and tungsten. The world-renowned large-scale gold-antimony-tungsten deposit, Hunan Woxi Gold Antimony Tungsten Deposit, is located in the northern section of this metallogenic belt [1, 2]. Numerous gold-polymetallic deposits (occurrences) scatter throughout the area, all of which are vein deposits. About 500 primary gold-polymetallic deposits (occurrences) have been discovered, including Woxi Gold Antimony Tungsten Deposit, Zhazixi Antimony Tungsten Deposit, Chanziping Gold Deposit, Pingcha Gold Antimony Deposit, Taojinzhong Gold Deposit, Dayetang Gold Deposit, Xingfengshan Gold Tungsten Deposit, Longshan Gold Antimony Tungsten Deposit and other large and medium-sized gold deposits, gold-antimony deposits, antimony-tungsten deposits, and gold-antimony-tungsten deposits [3, 4]. In recent years, significant progress has been made in the deep ore prospecting of gold deposits, such as Woxi, Huangjindong, and Wan'gu in the Xuefeng Mountain metallogenic belt, indicating that the metallogenic belt has superior ore-forming conditions and ore

prospecting prospects [5]. Due to the high mountains and dense forests in this area, the overall degree of geological work is low, and the ore-forming types are complex and diverse, which leads to great disputes on the source of ore-forming materials, hydrothermal solution and thermal power, as well as the ore-forming age, and the ore-forming laws of gold deposits in this area. In addition, although this area has invested a lot of human, material and financial resources, previous studies mainly focus on the deposit genesis and ore-forming mode of a single deposit or ore block, leading to no breakthrough in terms of ore prospecting results, especially new deposits.

The source of gold, antimony and tungsten ore-forming minerals and hydrothermal solution in the Xuefeng Mountain metallogenic belt has always been the focus of academic attention and controversy. For many typical deposits, such as Bake Gold Deposit, Pingqiu Gold Deposit, Mobin Gold Deposit, Zhazixi Antimony Tungsten Deposit, Woxi Gold Antimony Tungsten Deposit, and Longshan Gold Antimony Tungsten Deposit, many researchers have carried out tracer study of the source of gold, antimony, tungsten ore-forming minerals and hydrothermal solution using geochemical methods, such as trace elements, rare earth elements, S isotopes, Pb isotopes, H-O-C isotopes, and Sr isotopes, and formed different views accordingly. In terms of the source of

ore-forming materials, Liu et al. believed that the gold and antimony ore-forming materials came from the ore-hosting strata [6-8]; Peng et al. believed that the gold deposits may come from the deep strata, instead of the ore-hosting strata [9, 10]; Yang et al. [11] believed that the ore-forming materials of large-scale deposits, such as Woxi, Zhazixi, and Longshan, came from the ore-hosting strata, deep strata and even katathermal solution. In terms of the ore-forming hydrothermal solution source, Gu [12] believed through rock-water interaction simulation experiments that the ore-forming hydrothermal solution of gold deposits in southwestern Hunan was groundwater heated by magmatic rocks and tectonic forces; Gu et al. [13] believed that the ore-forming hydrothermal solution of the Woxi Gold Antimony Tungsten Deposit was mainly seawater, after studying the geology and fluid inclusions of the deposit and the geochemical characteristics of trace and rare earth elements; Zhu et al. [14] studied the noble gas isotopes of fluid inclusions using the laser Raman spectrometry, and the research results showed that the ore-forming hydrothermal solution of the Woxi Gold Antimony Tungsten Deposit was mainly deep hydrothermal solution, mixed with a small amount of atmospheric precipitation or groundwater; Zeng et al. [15] believed that the ore-forming hydrothermal solution of the Zhazixi Antimony Tungsten Deposit was a mixture of metamorphic and magmatic water after the isotope tracer study of H, O, and S; Liu [16] studied C, H, O, He-Ar, S and Pb of gold deposits in the Jiangnan orogenic belt, and the research results showed that the ore-forming hydrothermal solution mainly came from metamorphic and/or magmatic water, and also mantle fluids in the late ore-forming stage. In addition, the mantle or magmatic derived components were the source of ore-forming materials of gold-polymetallic deposits.

Although researchers have conducted some comprehensive research on the ore-forming hydrothermal solution of the Xuefeng Mountain [17], the existing studies have not fully recognized the ore-forming differences between the southern and northern sections. Both sections mainly produce gold, and have certain differences in some aspects, such as output structure, geological background, mineral and element association, which indicates that there may also be differences in the source of ore-forming materials and hydrothermal solution between both sections. Therefore, focusing on the ore-forming differences between both sections, this study analyzed the ore-forming hydrothermal components of gold-polymetallic deposits in both sections, which aimed to reveal their differences in the ore-forming hydrothermal solution source, and to fill the research gap in this area, thereby providing a basic theoretical basis for future scientific research work in this area.

This study compared and analyzed the ore-forming hydrothermal solution source using the characteristics of several aspects, such as ore bodies in both sections, fluid inclusions, hydrogen and oxygen isotopes, which aimed to provide basic support for making new breakthroughs in ore prospecting results in both sections.

2. REGIONAL BACKGROUND

The Xuefeng Mountain metallogenic belt is located in the metamorphic clastic rock type gold metallogenic belt of gold deposits in China [18] (Figure 1) on the southeast side of the southwest section of the Jiangnan axis, starting from the western margin of the Dongting fault depression in the east,

and ending in the northern Guangxi fold belt in the southwest. The Xuefeng Mountain metallogenic belt is divided into two parts, the Yangtze platform area in the northwest and the South China fold belt in the southeast, by the Anhua-Xupu-Jingzhou deep faults, crossing the two tectonic units of Yangtze platform and the South China fold system.

The exposed strata in the uplift area on the west side of the faults are mainly low-grade metamorphic clastic rocks, slate and volcanic tuff of the Lengjiaxi and Banxi Group, which are the basement strata with huge thickness. The Sinian, Cambrian, Carboniferous, Permian, Cretaceous and Tertiary strata overlap unconformity is above the basement strata. The Ordovician and Devonian strata are missing. The scattered strata distribution above the Carboniferous strata indicates that the area has been in a state of uplift for many times in the geological history [19].

Large folds are developed in the platform area on the west side of the faults. The faults are well-developed, some of which are tens of kilometers long, and mainly consist of two groups: NE-NNE and NW-near EW. The Xuefeng Mountain fold belt on the east side of the faults has steep strata, developed fold faults, and strong thrust nappe, forming a NNE tectonic belt.

The intermediate acid magmatic rocks in the platform area on the west side of the faults are not developed, with exposed granite batholith in Sanfang and Yuanbaoshan of northern Guangxi only. In the collage belt of Yangtze platform and South China fold system, many basic and ultra-basic rocks are exposed from Qianyang to Tongdao, which occur in the Banxi Group stratum in vein form in groups and belts, extending in the northeast direction [20]. The granites in the fold belt of the eastern margin of Xuefeng Mountain are widely exposed, and the diagenetic age ranges from the Caledonian to the Yanshanian period, with the Indosinian period as the main part.

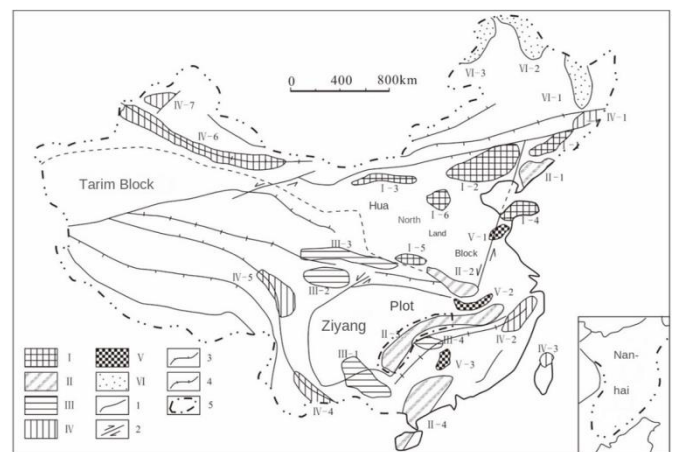


Figure 1. Location map of the gold metallogenic belt of the study area

Note: I. Greenstone type gold metallogenic belt; II. Metamorphic clastic rock type gold metallogenic belt; III. Sedimentary rock type gold metallogenic belt; IV. Volcanic rock type gold metallogenic belt; V. Granite type gold metallogenic belt; VI. Placer gold metallogenic belt; 1. Geological boundary; 2. Strike-slip fault 3. Plate overlap zone; 4. Plate docking zone; 5. Scope of the research area

3. CHARACTERISTICS OF FLUID INCLUSIONS

3.1 Samples and testing method

On the basis of detailed field and mineralogical

observations, this study totally collected 30 samples from Anjia and Bake Gold Deposit in the southern section of the Xuefeng Mountain metallogenic belt, and Zhazixi Antimony Tungsten Deposit and Woxi Gold Antimony Tungsten Deposit in the northern section, with all of them taken from the underground mother lode.

The petrographic observation of inclusions was carried out in the Key Laboratory of Nonferrous Metal Metallogenic Prediction of Ministry of Education in Central South University. According to the output characteristics and observation results of hand specimens, 20 samples were selected from the collected samples, and were ground into 0.3mm-thick double-sided polished inclusion thin sections. After petrographic observation of fluid inclusions, appropriate temperature measurement samples were selected and soaked in acetone. Then the thin sections were cleaned, and the homogenization freezing method was used for temperature measurement research and composition analysis. The temperatures of fluid inclusions were measured in the School of Geosciences and Info-physics, Central South University, using the Linkam-MDS600 cold and hot stage made in the UK as the fluid inclusion microscopic thermometer. The apparatus was set with a temperature control range of -196~500°C, a heating area of 22 mm, a heating rate of 0.01~150°C/min, and a precision of ±0.1°C.

Composition analysis of the inclusions was made in the Key Laboratory of Nonferrous Metal Metallogenic Prediction of Ministry of Education in Central South University. Gas phase composition analysis was made using the RG202 quadrupole mass spectrometer, with the repeatedly-measured precision less than 5%. Liquid phase composition analysis was made using HIC-6A ion chromatograph, with the repeatedly-measured precision less than 5%.

3.2 Petrographic characteristics of fluid inclusions

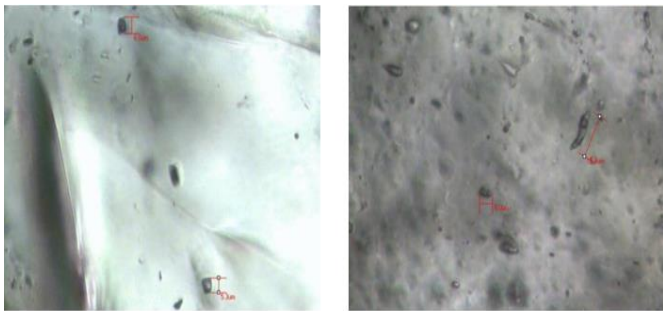


Figure 2. Testing diagrams of Anjia fluid inclusions

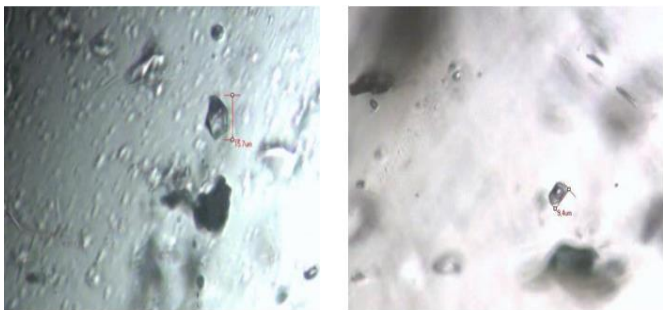


Figure 3. Testing diagrams of Bake fluid inclusions

Commonly developed in the ore-bearing quartz veins of Anjia, Bake, and Zhazixi, the fluid inclusions have different

sizes, with most of them being clustered or isolated primary inclusions. Based on the phase state of fluid inclusions at room temperature, and combined with the phase state changes during the temperature measurement process, quartz fluid inclusions were divided into three categories, namely, liquid rich type gas-liquid two-phase saline solution inclusions (type I), CO₂-containing three-phase inclusions (type II), and gas-liquid two-phase N₂ rich inclusions (type III). Only types I and II inclusions have been found in the Anjia and Bake gold deposits in the southern section (in Figures 2 and 3), while types I, II, and III inclusions are developed in the Zhazixi Antimony Tungsten Deposit in the northern section (in Figure 4).

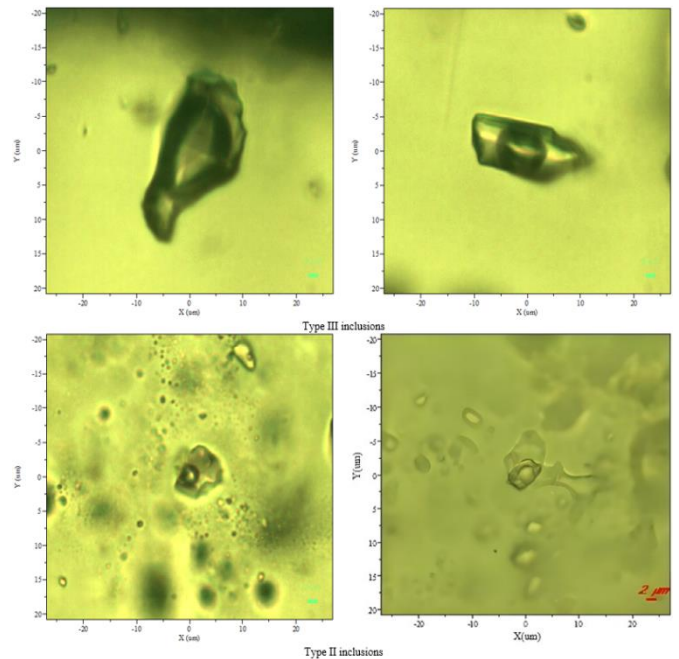


Figure 4. Testing diagrams of Zhazixi fluid inclusions

3.3 Composition characteristics of fluid inclusions

It can be seen from Tables 1 and 2 that the quartz fluid inclusions in the gold-polymetallic deposits in the study area have the following characteristics. The gas phase composition is mainly H₂O and CO₂, with H₂O content between 652μg·g⁻¹-3757μg·g⁻¹ and CO₂ content between 20.215μg·g⁻¹-804.000μg·g⁻¹. For the liquid phase composition, the main cations are Na⁺, Ca²⁺ and K⁺, with Na⁺ content between 0.210 μg·g⁻¹-24.700μg·g⁻¹, Ca²⁺ content between 0.420μg·g⁻¹-59.000μg·g⁻¹, and K⁺ content between 0.040μg·g⁻¹-27.200μg·g⁻¹. The main anions are Cl⁻ and SO₄²⁻, with Cl⁻ content between 0.095μg·g⁻¹-34.400μg·g⁻¹, and SO₄²⁻ content between 3.653μg·g⁻¹-53.005μg·g⁻¹. Overall, in the quartz fluid inclusions of gold-polymetallic deposits in the study area, ω (H₂O)>ω (CO₂)>ω (CH₄)>ω (H₂), ω (Na⁺)>ω (K⁺), ω (Ca²⁺)>ω (Mg²⁺), and ω (SO₄²⁻)>ω (Cl⁻)>ω (F⁻).

According to the Na-K-Ca triangular diagrams (Figures 5 and 6), the quartz fluid inclusions in gold deposits in the Xuefeng Mountain southern section are mainly Na⁺ and Ca²⁺, with K content much lower than Na and Ca content, indicating Na⁺-Ca²⁺ type. However, the quartz fluid inclusions in the Woxi Gold Antimony Tungsten Deposit in the northern section are located in two regions, which are Ca⁺ enriched type and Na⁺-K⁺-Ca²⁺ type.

Table 1. Gas phase composition content of quartz fluid inclusions in gold deposits in the study area (unit: $\mu\text{g}\cdot\text{g}^{-1}$)

| Original Sample Number | Location | H ₂ | N ₂ | CH ₄ | CO ₂ | H ₂ O | CO ₂ /H ₂ O | CO ₂ /(CH ₄ +H ₂) |
|------------------------|------------------|----------------|----------------|-----------------|-----------------|------------------|-----------------------------------|---|
| AJ-01 | | 0.259 | Trace | 2.734 | 43.894 | 1134.000 | 0.04 | 14.67 |
| AJ-02 | | 0.148 | Trace | 3.401 | 51.479 | 1210.000 | 0.04 | 14.51 |
| AJ-03 | | 0.044 | Trace | 1.539 | 46.572 | 925.000 | 0.05 | 29.42 |
| AJ-04 | | 0.075 | Trace | 1.437 | 20.215 | 857.000 | 0.02 | 13.37 |
| BK-01 | | 0.305 | Trace | 2.553 | 22.213 | 1034.000 | 0.02 | 7.77 |
| BK-02 | | 0.271 | Trace | 1.792 | 31.467 | 1078.000 | 0.03 | 15.25 |
| BK-03 | | 0.174 | Trace | 2.407 | 37.263 | 1142.000 | 0.03 | 14.44 |
| BK-04 | | 0.092 | Trace | 1.924 | 30.824 | 1285.000 | 0.02 | 15.29 |
| BK-05 | | 0.270 | Trace | 3.059 | 28.735 | 1056.000 | 0.03 | 8.63 |
| BK-06 | | 0.193 | Trace | 2.920 | 34.792 | 1182.000 | 0.03 | 11.18 |
| XJ-1 | Southern section | 0.580 | Trace | 1.523 | 80.327 | 652.000 | 0.12 | 38.20 |
| XJ-2 | | 0.073 | 0.025 | 1.664 | 89.263 | 1034.000 | 0.09 | 51.39 |
| XJ-3 | | 0.734 | 0.015 | 3.059 | 80.526 | 1216.000 | 0.07 | 21.23 |
| XJ-4 | | 0.625 | 0.011 | 2.735 | 81.256 | 1102.000 | 0.07 | 24.18 |
| XJ-5 | | 0.193 | Trace | 1.849 | 92.563 | 920.000 | 0.10 | 45.33 |
| YWT-1 | | 0.593 | Trace | 4.188 | 66.340 | 980.000 | 0.07 | 13.88 |
| YWT-2 | | 0.329 | Trace | 3.850 | 68.256 | 994.000 | 0.07 | 16.33 |
| YWT-3 | | 0.199 | / | 2.678 | 59.254 | 1021.000 | 0.06 | 20.60 |
| YWT-4 | | 0.085 | / | 3.643 | 64.354 | 1005.000 | 0.06 | 17.26 |
| YWT-5 | | 0.094 | / | 4.312 | 63.847 | 1015.000 | 0.06 | 14.49 |
| YWT-6 | | 0.235 | / | 2.450 | 69.788 | 1214.000 | 0.06 | 25.99 |
| WX-1 (outside) | | 1.290 | 24.010 | Trace | 290.627 | 2094.000 | 0.14 | / |
| WX-2 (outside) | | 0.190 | 129.230 | 1.470 | 247.772 | 2010.000 | 0.12 | 149.26 |
| WX-3 (outside) | | 1.660 | 50.530 | Trace | 294.777 | 2252.000 | 0.13 | / |
| WX-4 (outside) | | 0.800 | 30.270 | Trace | 99.834 | 1711.000 | 0.06 | / |
| WX-5 (outside) | | 0.380 | 31.070 | Trace | 74.203 | 1551.000 | 0.05 | / |
| WX-6 (outside) | | 0.340 | 61.490 | Trace | 74.208 | 2775.000 | 0.03 | / |
| WX-7 (outside) | | 0.380 | 25.950 | Trace | 66.589 | 1010.000 | 0.07 | / |
| WX-8 (outside) | | 0.440 | 51.670 | Trace | 64.980 | 1851.000 | 0.04 | / |
| WX-9 (outside) | | 0.410 | 30.290 | 0.730 | 47.521 | 1575.000 | 0.03 | 41.69 |
| WX-10 (outside) | | 0.400 | 44.190 | 0.480 | 37.829 | 1073.000 | 0.04 | 42.99 |
| WX-11 (rich) | Northern section | 0.100 | 7.400 | 0.280 | 142.000 | 2620.000 | 0.05 | 373.68 |
| WX-12 (rich) | | 0.200 | 17.500 | 0.500 | 142.000 | 2850.000 | 0.05 | 202.86 |
| WX-13 (rich) | | 0.200 | 14.400 | 0.200 | 88.000 | 2180.000 | 0.04 | 220.00 |
| WX-14 (rich) | | 0.200 | 8.800 | 0.400 | 88.000 | 2800.000 | 0.03 | 146.67 |
| WX-15 (rich) | | 0.400 | / | Trace | 316.480 | 3757.000 | 0.08 | / |
| WX-16 (poor) | | 0.300 | 3.800 | 0.600 | 34.000 | 2240.000 | 0.02 | 37.78 |
| WX-1 | | / | 0.074 | 24.736 | 344.640 | 1615.000 | 0.21 | / |
| WX-2 | | / | Trace | 3.266 | 128.830 | 1072.000 | 0.12 | / |
| WX-3 | | / | Trace | 9.125 | 405.270 | 987.000 | 0.41 | / |
| WX-4 | | / | 0.053 | 10.860 | 804.000 | 856.000 | 0.94 | / |
| WX-5 | | / | 0.038 | 10.886 | 781.420 | 1993.000 | 0.39 | / |

Notes: "AJ" means Anjia, and "BK" means Bake, with both data coming from this study, and the School of Geosciences and Info-physics in Central South University as the testing organization; "XJ" means Xiaojia, "YWT" means Yangwantuan, and "WX" means Woxi.

Table 2. Liquid phase composition content of quartz fluid inclusions in gold deposits in the study area (unit: $\mu\text{g}\cdot\text{g}^{-1}$)

| Original Sample Number | Location | F ⁻ | Cl ⁻ | SO ₄ ²⁻ | Na ⁺ | K ⁺ | Mg ²⁺ | Ca ²⁺ | Na ⁺ /K ⁺ | Cl ⁻ /F ⁻ |
|------------------------|------------------|----------------|-----------------|-------------------------------|-----------------|----------------|------------------|------------------|---------------------------------|---------------------------------|
| AJ-01 | | 0.417 | 4.051 | 7.489 | 4.325 | 0.789 | 0.103 | 5.325 | 5.48 | 9.71 |
| AJ-02 | | 0.285 | 3.805 | 13.052 | 3.824 | 0.953 | 0.041 | 6.643 | 4.01 | 13.35 |
| AJ-03 | | 0.604 | 5.417 | 8.536 | 4.016 | 0.529 | 0.082 | 4.627 | 7.59 | 8.97 |
| AJ-04 | | 0.545 | 1.537 | 8.429 | 6.218 | 1.044 | 0.110 | 6.701 | 5.96 | 21.28 |
| BK-01 | | 0.128 | 2.724 | 5.478 | 5.420 | 0.693 | Trace | 7.264 | 7.82 | 5.89 |
| BK-02 | | 0.259 | 1.526 | 9.117 | 7.534 | 1.247 | 0.075 | 9.429 | 6.04 | 5.69 |
| BK-03 | | 0.324 | 1.845 | 7.593 | 8.305 | 0.899 | Trace | 8.517 | 9.24 | 13.98 |
| BK-04 | | 0.153 | 2.139 | 10.140 | 6.447 | 1.107 | 0.098 | 6.492 | 5.82 | 13.58 |
| BK-05 | | 0.275 | 3.735 | 6.904 | 7.105 | 0.657 | 0.051 | 8.349 | 10.81 | 12.69 |
| BK-06 | | 0.228 | 2.894 | 5.628 | 3.571 | 0.459 | 0.063 | 4.593 | 7.78 | 2.82 |
| XJ-1 | Southern section | 0.385 | 0.875 | 6.188 | 2.060 | 4.043 | 0.108 | 1.200 | 0.51 | 2.27 |
| XJ-2 | | 0.056 | 1.705 | 53.005 | 9.178 | 4.065 | 0.898 | 6.240 | 2.26 | 30.45 |
| XJ-3 | | 0.052 | 2.503 | 9.873 | 3.948 | 1.940 | 0.238 | 3.113 | 2.04 | 48.13 |
| XJ-4 | | 0.050 | 3.280 | 11.465 | 3.248 | 3.240 | 0.223 | 1.853 | 1.00 | 65.60 |
| XJ-5 | | 0.450 | 0.095 | 3.653 | 5.725 | 1.045 | 0.123 | 1.738 | 5.48 | 0.21 |
| YWT-1 | | 0.466 | 17.928 | 8.856 | 16.734 | 0.409 | 0.250 | 2.959 | 40.91 | 38.47 |
| YWT-2 | | 0.515 | 1.613 | 4.058 | 2.728 | 0.428 | 0.310 | 1.985 | 6.37 | 3.13 |
| YWT-3 | | 0.063 | 4.441 | 7.103 | 4.606 | 0.631 | 0.463 | 2.853 | 7.30 | 70.49 |
| YWT-4 | | 0.071 | 3.900 | 4.950 | 4.154 | 0.381 | 0.207 | 2.557 | 10.90 | 54.93 |
| YWT-5 | | 0.455 | 3.473 | 10.693 | 4.063 | 0.885 | 0.715 | 2.718 | 4.59 | 7.63 |

| | | | | | | | | | | |
|----------------|------------------|-------|--------|--------|--------|--------|-------|--------|-------|-------|
| YWT-6 | | 0.878 | 3.605 | 5.058 | 4.175 | 0.250 | 1.988 | 2.395 | 16.70 | 4.11 |
| WX-1 (outside) | | 1.500 | 1.530 | / | 0.510 | 0.100 | 0.040 | 2.160 | 5.10 | 1.02 |
| WX-2 (outside) | | 1.160 | 4.300 | / | 0.520 | 0.210 | 0.040 | 1.100 | 2.48 | 3.71 |
| WX-3 (outside) | | 1.620 | 3.820 | / | 0.400 | 0.040 | 0.040 | 0.430 | 10.00 | 2.36 |
| WX-4 (outside) | | 1.180 | 2.420 | / | 0.300 | 0.100 | 0.090 | 0.420 | 3.00 | 2.05 |
| WX-5 (outside) | | 1.430 | 2.700 | / | 0.200 | 0.120 | 0.040 | 2.180 | 1.67 | 1.89 |
| WX-6 (outside) | | 1.380 | 2.790 | / | 0.300 | 0.160 | 0.090 | 2.100 | 1.88 | 2.02 |
| WX-7 (outside) | | 1.220 | 3.080 | / | 1.120 | 0.200 | 0.020 | 2.170 | 5.60 | 2.52 |
| WX-8 (outside) | | 1.450 | 1.000 | / | 0.210 | 0.040 | 0.060 | 1.130 | 5.25 | 0.69 |
| WX-9 (outside) | | 1.310 | 2.710 | / | 0.210 | 0.100 | 0.020 | 2.180 | 2.10 | 2.07 |
| WX-10 (rich) | Northern section | 2.100 | 24.000 | / | 24.700 | 17.800 | 1.500 | 10.500 | 1.39 | 11.43 |
| WX-11 (rich) | | 1.900 | 34.400 | / | 18.200 | 17.400 | 6.700 | 12.800 | 1.05 | 18.11 |
| WX-12 (rich) | | 1.500 | 25.000 | / | 17.200 | 20.800 | 4.600 | 12.800 | 0.83 | 16.67 |
| WX-13 (rich) | | 1.700 | 14.100 | / | 21.900 | 9.200 | 0.400 | 7.800 | 2.38 | 8.29 |
| WX-14 (poor) | | 1.500 | 22.500 | / | 18.400 | 27.200 | 7.400 | 59.000 | 0.68 | 15.00 |
| WX-1 | | 0.178 | 1.724 | 42.963 | 2.496 | 5.627 | Trace | 10.255 | 0.44 | 9.69 |
| WX-2 | | 0.053 | 2.059 | 46.674 | 5.490 | 3.782 | Trace | 2.524 | 1.45 | 38.85 |
| WX-3 | | 0.412 | 11.911 | 44.529 | 1.877 | 1.674 | 1.503 | 4.983 | 1.12 | 28.91 |
| WX-4 | | 0.182 | 13.029 | 10.975 | 1.271 | 1.047 | 3.479 | 4.196 | 1.21 | 71.59 |
| WX-5 | | 0.273 | 9.333 | 37.418 | 2.434 | 0.842 | 1.271 | 5.842 | 2.89 | 34.19 |

Notes: "AJ" means Anjia, and "BK" means Bake, with both data coming from this study, and the School of Geosciences and Info-physics in Central South University as the testing organization; "XJ" means Xiaojia, "YWT" means Yangwantuan, "WX" means Woxi.

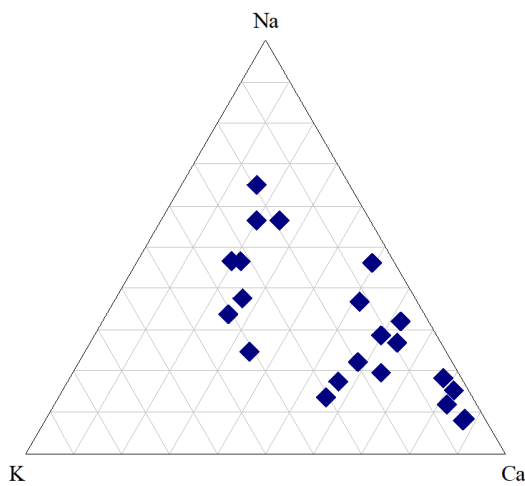


Figure 5. Na-K-Ca diagram of fluid inclusions in the Woxi Gold Antimony Tungsten Deposit

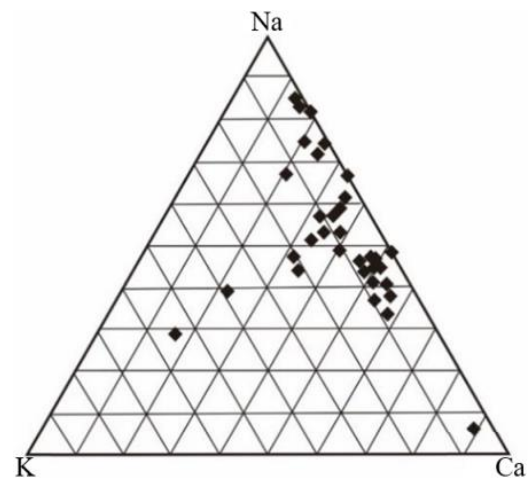


Figure 6. Na-K-Ca diagram of fluid inclusions in the southern deposits of the study area

4. CHARACTERISTICS OF HYDROGEN AND OXYGEN ISOTOPES

4.1 Samples and testing method

Samples were collected from representative samples in the main ore-forming stages of each deposit. The hydrogen and oxygen isotope method was described in detail. For hydrogen isotopes of fluid inclusions, water was obtained using the decrepitation method, and the sample was placed in a high-temperature resistant vessel. After vacuating the vessel, the sample was heated. When the temperature reached the decrepitation temperature of the inclusion, the inclusion decrepitated. H₂O was collected after being released after the inclusion decrepitation, and then zinc metal was used as the reducing agent to produce hydrogen. For oxygen isotopes, the strong oxidant BrF₅ was used for oxidation to collect pure O₂ from quartz and produce CO₂. The international standard SMOW was adopted for hydrogen and oxygen isotopes, while the national standard PDB was adopted for carbon isotopes, with ±0.2‰ as the carbon and oxygen isotope analysis accuracy, and ±0.2‰ as the hydrogen isotope analysis accuracy.

4.2 Characteristics of hydrogen and oxygen isotopes

According to Table 3, for the quartz fluid inclusions in sulfur poor quartz vein type single gold deposits in the southern section of the Xuefeng Mountain metallogenic belt, δD_{H₂O} is between -114.5~-38, with a range of 76.5 and an average of -81.65; δ¹⁸O_{H₂O} is between -2~6.98, with a range of 8.98 and an average of 3.66. For quartz fluid inclusions in sulfur rich altered fracture zone type single gold deposits in the middle section, δD_{H₂O} is between -102.3~-45.6, with a range of 56.7 and an average of -68.66; δ¹⁸O_{H₂O} is between 0.79~8.62, with a range of 7.83 and an average of 5.46. For quartz fluid inclusions the Zhazixi Antimony Tungsten Deposit in the middle section, δD_{H₂O} is between -78~-49, with a range of 29 and an average of -61.60; δ¹⁸O_{H₂O} is between 3.5~7.4, with a range of 2.9 and an average of 5.84. For quartz fluid inclusions in the Woxi Gold Antimony Tungsten Deposit in the northern section, δD_{H₂O} is between -85.92~-54.99, with a range of 30.93 and an average of -58.25; δ¹⁸O_{H₂O} is between 4.22~15.02, with a range of 10.8 and an average of 6.73. In the Xuefeng Mountain gold-polymetallic metallogenic belt, δD_{H₂O} and δ¹⁸O_{H₂O} of gold, antimony-tungsten, and gold-antimony-tungsten deposits show an increasing trend from south to north.

Table 3. Hydrogen and oxygen isotope content of single quartz mineral in gold deposits in the study area (‰)

| Sample Number | Orefield (Location) | δD_{H_2O} | $\delta^{18}O_{quartz}$ | $\delta^{18}O_{H_2O}$ | Sample Number | Orefield (Location) | δD_{H_2O} | $\delta^{18}O_{quartz}$ | $\delta^{18}O_{H_2O}$ |
|---------------|--------------------------------|-------------------|-------------------------|-----------------------|---------------|-----------------------------|-------------------|-------------------------|-----------------------|
| AJ-01 | | -95.50 | 15.40 | 1.27 | CZP-8 | | -56.00 | 16.34 | 5.89 |
| AJ-02 | Anjia (southern section) | -105.70 | 16.00 | 1.87 | CZP-9 | | -79.00 | 11.24 | 0.79 |
| AJ-03 | | -114.50 | 17.90 | 3.77 | CZP-10 | | -59.00 | 14.28 | 3.83 |
| AJ-04 | | -113.40 | 18.30 | 6.98 | CZP-11 | | -70.10 | 16.25 | 6.80 |
| AJ-05 | | -111.30 | 16.40 | 2.27 | CZP-12 | | -64.30 | 16.35 | 8.62 |
| BK-01 | Bake (southern section) | -91.00 | 15.20 | 2.14 | CZP-13 | Chanziping (middle section) | -54.70 | 16.58 | 7.14 |
| BK-02 | | -97.10 | 17.50 | 4.44 | CZP-14 | | -45.60 | 16.36 | 1.06 |
| BK-03 | | -99.80 | 17.30 | 4.24 | CZP-15 | -102.30 | 14.70 | 4.30 | |
| BK-04 | | -100.20 | 16.90 | 3.84 | CZP-16 | -100.60 | 14.40 | 5.90 | |
| BK-05 | | -109.00 | 17.20 | 4.14 | CZP-17 | -80.60 | 15.70 | 7.20 | |
| BK-06 | | -112.20 | 17.40 | 4.34 | CZP-18 | -72.60 | 16.33 | 7.80 | |
| PC-1 | Pingcha (southern section) | -65.00 | 17.50 | 5.20 | CZP-19 | | -50.60 | 15.50 | 7.00 |
| PC-2 | | -58.00 | 17.50 | 5.30 | CZP-20 | | -66.60 | 15.40 | 6.90 |
| PC-3 | | -52.00 | 16.90 | 4.80 | ZZX-1 | Zhazixi (middle section) | -68.00 | 17.90 | 6.20 |
| PC-4 | | -59.00 | 16.70 | 3.70 | ZZX-2 | | -57.00 | 19.10 | 7.40 |
| PC-5 | | -38.00 | 16.90 | 3.30 | ZZX-3 | | -49.00 | 15.20 | 3.50 |
| TJC-1 | Taojinchong (southern section) | -44.00 | 20.70 | 8.90 | ZZX-4 | | -56.00 | 17.30 | 5.60 |
| TJC-2 | | -50.00 | 20.00 | 7.90 | ZZX-5 | | -78.00 | 18.20 | 6.50 |
| TJC-3 | | -81.00 | 19.00 | 3.80 | WX-1 | Woxi (northern section) | -54.99 | 26.10 | 15.02 |
| TJC-4 | | -63.00 | 19.40 | 4.20 | WX-2 | | -58.35 | 16.30 | 5.22 |
| TJC-5 | | -62.00 | 19.50 | 3.20 | WX-3 | | -85.92 | 18.30 | 7.22 |
| TJC-6 | | -70.00 | 18.20 | 1.00 | WX-4 | | -64.00 | 16.50 | 5.42 |
| TJC-7 | | -82.00 | 16.40 | -0.80 | WX-5 | | -81.00 | 17.40 | 6.32 |
| TJC-8 | | -86.00 | 16.50 | -2.00 | WX-6 | | -69.00 | 15.70 | 4.62 |
| CZP-1 | -70.10 | 16.25 | 6.81 | WX-7 | -64.00 | | 15.30 | 4.22 | |
| CZP-2 | -64.30 | 16.35 | 6.91 | WX-8 | -64.00 | | 16.50 | 5.42 | |
| CZP-3 | Chanziping (middle section) | -54.70 | 16.58 | 7.14 | WX-9 | -64.00 | 18.20 | 7.12 | |
| CZP-4 | | -91.20 | 15.80 | 5.35 | WX-10 | -118.00 | 17.80 | 6.72 | |
| CZP-5 | | -58.00 | 15.07 | 4.62 | WX-11 | -69.00 | 15.70 | 4.62 | |
| CZP-6 | | -77.00 | 11.58 | 1.13 | WX-12 | -81.00 | 17.40 | 6.32 | |
| CZP-7 | | -56.00 | 14.45 | 4.00 | | | | | |

5. DISCUSSION

5.1 Implications of fluid inclusions on the ore-forming hydrothermal solution source

Previous studies [21] have shown that the ratio of different ions in the liquid phase composition of fluid inclusions reflects the fluid source to some extent. For example, $F-/Cl-<1$ reflects that the ore-forming fluids come from formation fluids or atmospheric precipitation; $K+/Na+>1$ reflects that the possibility of the ore-forming fluids coming from magmatic water is relatively high; $K+/Na+<1$ reflects that the ore-forming fluids are either magmatic water or other hydrothermal solution. According to the fluid inclusion characteristics (Tables 1 and 2) of deposits in typical late Caledonian-early Indosinian period, such as Bake, Anjia, Pingcha, and Yangwantuan, $K+/Na+<1$ and $F-/Cl-<1$ in the quartz fluid inclusions of gold deposits in the southern section reflect that the ore-forming fluids may come from formation fluids or atmospheric precipitation, instead of magmatic water. At the same time, there are neither intermediate acid magmatic

rocks exposed in the ore-forming concentration area in the Xuefeng Mountain southern section, nor dome structure or alteration characteristics caused by magmatic activity. Geophysical data shows that there is no concealed rock mass in the deep, which further confirms that the ore-forming hydrothermal solution during the period comes from formation fluids or atmospheric precipitation, instead of magmatic water.

The cations in the fluid inclusions of the southern gold deposits are mainly Na^+ and Ca^{2+} , while the anions are mainly SO_4^{2-} and Cl^- . The high Ca^{2+} content suggests that groundwater may be involved. Comparison results of groundwater in the area show that the bedrock fissure water in the Banxi Group stratum is mainly $HCO_3 \cdot Cl-Na \cdot Ca$ type and $HCO_3-Na \cdot Ca$ type. In addition, the groundwater in the Mobin Gold Deposit is HCO_3-Na (15m underground), $HCO_3-Na \cdot Ca$ (55m underground), $HCO_3 \cdot SO_4-Ca$ (75m underground), $SO_4 \cdot HCO_3-Ca$ (120m underground), and $SO_4-Ca \cdot Na$ (140m underground) one by one from shallow to deep (Army 00939, 1978). The composition of fluid inclusions is very similar to

that of groundwater in the area, indicating that groundwater plays an important role during the ore-forming period.

According to the Na-K-Ca diagrams (Figures 5 and 6), the sample distribution of the Woxi Gold Antimony Tungsten Deposit, which is the typical deposit in the northern section, is significantly different from that of the gold deposits in the southern section, suggesting that the ore-forming hydrothermal solution source of gold-polymetallic deposits in the Xuefeng Mountain northern section is different from that of gold deposits in the southern section.

According to the characteristics of fluid inclusions, the CO₂ and N₂ content in the gas phase composition of the fluid inclusions in the Woxi Gold Antimony Tungsten Deposit in the northern section is much higher than that of gold deposits in the southern section. CO₂ and N₂ are often deep source gases, therefore, the fluids with high CO₂ are generally believed to come from three possible sources, namely, magmatic hydrothermal solution, mantle source, and high-grade metamorphic fluids in the lower crust [22-24]. Although it cannot be determined the fluids with high CO₂ in the Woxi Gold Antimony Tungsten Deposit come from which of the three sources, it can be determined that the fluids in the deeper source are involved in the ore forming. N₂ is one of the important components of fluid inclusions in some eclogite, granulite and low-grade metamorphic sedimentary rocks [25]. The low-grade metamorphic Banxi Group clastic rocks are widely exposed in the area, and the stratum is rich in organic carbon, which has the potential to provide a large amount of N₂. However, decomposition reaction of organic matter occurs in the stratum rich in organic matter in the low-grade metamorphic environment, which usually forms low-grade metamorphic fluids dominated by N₂ and CH₄. But CH₄ in quartz fluid inclusions of gold deposits in the north section is

very low. Therefore, the main source of N₂ in fluid inclusions is not the epimetamorphism of wall rocks. At present, inclusions rich in N₂ have been found in ultrahigh pressure metamorphic fluids only. So far, 0~100mol% N₂-dominated and pure N₂ inclusions have been found in spinel dunite xenoliths in Lanzarote in Canary Islands only. Therefore, it is inferred that N₂ in fluid inclusions of gold deposits in the northern section is from the deep source.

5.2 Implications of ore body characteristics on the ore-forming hydrothermal solution source

There are certain differences in gold deposits in the southern and northern sections of the Xuefeng Mountain metallogenic belt in several aspects, such as output structure, geological background, mineral and element association, which indicate that there may also be differences in the source of ore-forming materials and hydrothermal solution between both sections.

The southern section is mainly composed of single gold deposits with poor sulfides. The gold ore body type is mainly the quartz vein type in the NE-NNE direction mostly (Table 4). The gold mineral is mainly native gold as shown in Figure 7 (Photos 1 to 4), and is mostly exposed gold, such as Bake Gold Deposit, Jinjing Gold Deposit, Anjia Gold Deposit, Pingqiu Gold Deposit, and Mobin Gold Deposit. The accessory minerals are mainly pyrrhotite, followed by arsenopyrite. The subhedral-euhedral crystal form is good, occurring in lumps. The quartz vein is mostly milky white and often relatively pure, indicating that the ore-forming hydrothermal solution source in the southern region is relatively single and the solution composition is relatively simple.

Table 4. Ore-forming age and ore body characteristics of typical deposits in the Xuefeng Mountain metallogenic belt

| Orefiled Name | Location | Type of Gold Ore Body | Strike of Gold (Antimony) Ore Body |
|---|------------------|--|------------------------------------|
| Pingcha Gold Deposit | Southern section | Sulfur poor quartz vein type | Near EW |
| Tonggu Gold Deposit | Southern section | Sulfur poor quartz vein type | NE |
| Bake Gold Deposit | Southern section | Sulfur poor quartz vein type | NE |
| Pingqiu Gold Deposit | Southern section | Sulfur poor quartz vein type | NE |
| Jinjing Gold Deposit | Southern section | Sulfur poor quartz vein type | NE |
| Yangwantuan Gold Deposit | Southern section | Sulfur poor quartz vein type | NE |
| Jinliangchong Gold Deposit | Southern section | Sulfur poor quartz vein type | NE |
| Jintou Gold Deposit | Southern section | Sulfur poor quartz vein type | NE |
| Mobin Gold Deposit | Southern section | Sulfur poor quartz vein type | NE |
| Xiaojia Gold Deposit | Southern section | Sulfur poor quartz vein type | Near SN |
| Daping Gold Deposit | Middle section | Sulfur rich altered fracture zone type | NW |
| Chanziping Gold Deposit | Middle section | Sulfur rich altered fracture zone type | NW |
| Longshan Gold Antimony Tungsten Deposit | Middle section | Sulfur rich quartz veinlet zone type | Near EW |
| Xiejiashan Gold Antimony Deposit | Middle section | Sulfur rich quartz veinlet zone type | Near EW |
| Zhazixi Antimony Tungsten Deposit | Northern section | Sulfur rich quartz veinlet zone type | NW (antimony) |
| Woxi Gold Antimony Tungsten Deposit | Northern section | Gold-antimony-tungsten bearing quartz vein type and gold-bearing fractured altered rock type | Near EW-NW |
| Liulincha Gold Deposit | Northern section | Sulfur poor albite-quartz vein type | NEE |
| Shenjiaya Gold Deposit | Northern section | Sulfur poor and gold-bearing quartz vein type and structural altered rock type | Near EW |

In the middle and northern sections, the sulfide content increases, and the ore mineral association changes from single gold deposits to polymetallic deposits, such as gold-antimony, gold-antimony-tungsten, and antimony-tungsten. The gold mineral is mainly native gold, with micro gold or enclosed

very fine gold particle as the main type. The main ore body types are quartz veinlet zones and altered fracture zones. The main ore body is in the NW-near EW direction (Table 4), such as Daping Gold Deposit, Zhuanziping Gold Deposit, and Zhazixi Antimony Tungsten Deposit. The accessory minerals

are mainly pyrrhotite, followed by arsenopyrite, accompanied by a small amount of wolframite and sphalerite. The subhedral-euhedral crystal form is poor. The quartz vein is mostly smoky gray, indicating that the ore-forming hydrothermal solution in the middle and northern sections is relatively complex.

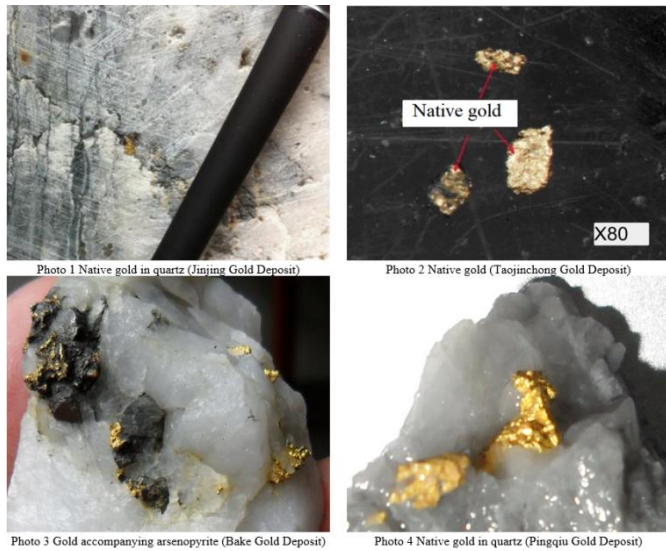


Figure 7. Native gold in gold minerals

5.3 Implications of isotope characteristics on the ore-forming hydrothermal solution source

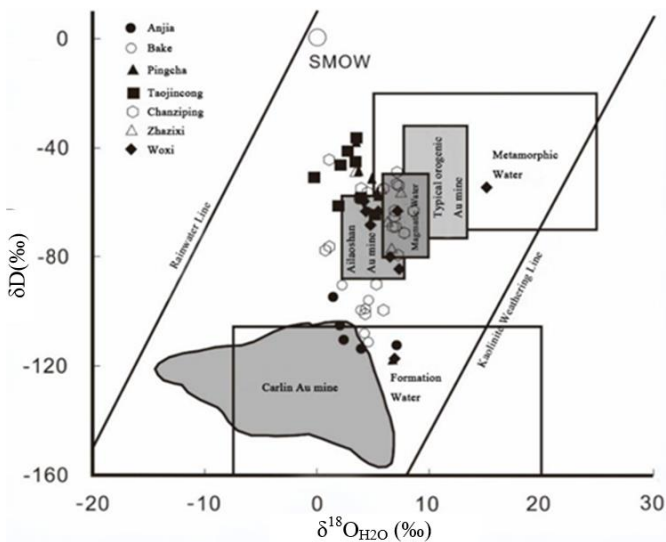


Figure 8. $\delta D-\delta^{18}O_{H_2O}$ diagram of typical deposit fluid inclusions in the Xuefeng Mountain metallogenic belt

Hydrogen and oxygen isotopes are often used to trace the source areas of ore-forming fluids in hydrothermal deposits, and the ore-forming process of hydrothermal vein type deposits is essentially a process of fluid interaction. H and O isotopes of the ore-forming fluids of deposits in the Xuefeng Mountain southern section (e.g. Bake Gold Deposit, Anjia Gold Deposit, Pingcha Gold Antimony Deposit, and Taojinchong Gold Deposit) are somewhat different from those in the middle and northern sections (e.g. Chanziping Gold Deposit, Zhazixi Antimony Tungsten Deposit, and Woxi Gold

Antimony Tungsten Deposit). In the $\delta D-\delta^{18}O_{H_2O}$ isotope diagram (Figure 8), the samples of the Bake and Anjia Gold Deposit in the anticlinal prostration space both fall within and near the range of the formation water, and are close to the distribution range of the Carlin type gold deposits. They are far from metamorphic and magmatic water, indicating that the ore-forming hydrothermal solution of the ore body mainly comes from the formation water, mixed with a small amount of atmospheric precipitation. The samples of Pingcha Gold Antimony Deposit and Taojinchong Gold Deposit in the shear zone quartz vein type mainly fall into the vicinity of metamorphic water. The samples of Chanziping Gold Deposit, Zhazixi Antimony Tungsten Deposit and Woxi Gold Antimony Tungsten Deposit mainly fall into metamorphic and magmatic water and their overlap area, which is consistent with collisional orogenic type gold deposits in the Ailao Mountain in Yunnan, suggesting that they may come from the same fluid source, i.e., metamorphic and magmatic water.

6. CONCLUSION

Based on the ore-forming differences between the northern and southern sections of the Xuefeng Mountain metallogenic belt, and combined with fluid inclusion characteristics and hydrogen and oxygen isotope testing results, this study believes that the ore-forming hydrothermal solution of gold deposits in the southern section mainly comes from groundwater, and that of gold-polymetallic deposits in the northern section comes from a mixture of magmatic rocks, metamorphic water, and groundwater. The main arguments are as follows:

(1) The gold deposits in the Xuefeng Mountain metallogenic belt gradually transform from sulfur poor single gold deposits to sulfur rich gold-antimony deposits and gold-antimony-tungsten deposits from south to north, indicating that the ore-forming hydrothermal solution gradually becomes complex from south to north.

(2) The quartz fluid inclusions of gold deposits in the southern section have high Ca^{2+} content, with $K^+/Na^+ < 1$ and $F/Cl < 1$, which is similar to the characteristics of groundwater in the study area. In addition, the gas composition has extremely low CO_2 and N_2 content, and its hydrogen and oxygen isotopes mainly fall near the formation and metamorphic water in the $\delta D-\delta^{18}O_{H_2O}$ isotope diagram. At the same time, the ore forming of gold deposits in the southern section is single, and the metal accessory minerals are relatively simple. The above characteristics show that the ore-forming hydrothermal solution of gold deposits in the Xuefeng Mountain southern section mainly comes from groundwater;

(3) For the quartz fluid inclusions of gold-polymetallic deposits in the northern section, the cation composition is Ca^+ enriched type and $Na^+-K^+-Ca^{2+}$ type, which is significantly different from the Na^+-Ca^{2+} type in the southern section. The gas composition has high CO_2 and N_2 content, and pure N_2 inclusions are developed, indicating deep source characteristics. The hydrogen and oxygen isotopes mainly fall in metamorphic and magmatic water and their overlap area in the $\delta D-\delta^{18}O_{H_2O}$ isotope diagram. In addition, the ore-forming characteristics of high sulfur gold-polymetallic deposits indicate that the ore-forming hydrothermal solution comes from the mixture of magmatic rocks, metamorphic water and groundwater.

FUNDINGS

This paper was supported by Hunan Provincial Natural Science Foundation of China (Grant No.: 2023JJ50339); Zunyi Normal University Academic New Seedling Cultivation Project (Zunshi XM [2021] Grant No.: 1-07); Zunyi Normal University 2021 Rural Revitalization Project (Jianjiaohe KY [2016] Grant No.: 018-5) and the doctoral fund project of Zunyi Normal University (Zunyi Normal University BS [2019] Grant No.: 08).

REFERENCES

- [1] Andersen, T., Whitehouse, M.J., Burke, E.A.J. (1997). Fluid inclusions in Scourian granulites from the Lewisian complex of NW Scotland: Evidence for CO₂-rich fluid in Late Archean high-grade metamorphism. *Lithos*, 40(2-4): 93-104. [https://doi.org/10.1016/S0024-4937\(97\)00005-4](https://doi.org/10.1016/S0024-4937(97)00005-4)
- [2] Taylor, B.E. (1986). Magmatic volatiles; isotopic variation of C, H, and S. *Reviews in Mineralogy and Geochemistry*, 16(1): 185-225. <https://doi.org/10.1515/9781501508936-012>
- [3] Beaudoin, G., Pitre, D. (2005). Stable isotope geochemistry of the Archean Val-d'Or (Canada) orogenic gold vein field. *Mineralium Deposita*, 40: 59-75. <https://doi.org/10.1007/s00126-005-0474-z>
- [4] Andersen, T., Burke, E.A.J., Neumann, E.R. (1995). Nitrogen-rich fluid in the upper mantle: Fluid inclusions in spinel dunite from Lanzarote, Canary Islands. *Contributions to Mineralogy and Petrology*, 120(1): 20-28. <https://doi.org/10.1007/BF00311005>
- [5] Kretschmar, U., McBride, D. (2016). The metallogeny of lode gold deposits: A syngenetic perspective. *Geoscience Canada*, 43(4): 291-293. <https://doi.org/10.12789/geocanj.2016.43.112>
- [6] Ashchepkov, I.V., Ntaflos, T., Spetsius, Z.V., Salikhov, R.F., Downes, H. (2017). Interaction between protokimberlite melts and mantle lithosphere: Evidence from mantle xenoliths from the Dalnyaya kimberlite pipe, Yakutia (Russia). *Geoscience Frontiers*, 8(4): 693-710. <https://doi.org/10.1016/j.gsf.2016.05.008>
- [7] Zhou, Z., Yonezu, K., Imai, A., Tindell, T., Li, H., Gabo-Ratio, J.A. (2022). Trace elements mineral chemistry of sulfides from the Woxi Au-Sb-W deposit, southern China. *Resource Geology*, 72(1): e12279. <https://doi.org/10.1111/rge.12279>
- [8] Zhang, P., Tang, P.K., Chen, A.Q. (2019). The evidences of sulfur isotope geochemistry for the source of metallogenic substance in the Woxi Au-Sb-W deposit. *Mineral Exploration*, 10(3): 530-536. <https://doi.org/10.3969/j.issn.1674-7801.2019.03.016>
- [9] Peng, J.T., Hu, R.Z., Zhao, J.H., Fu, Y.Z., Lin, Y.X. (2003). Scheelite Sm-Nd dating and quartz Ar-Ar dating for Woxi Au-Sb-W deposit, western Hunan. *Science Bulletin*, 48(23): 2640-2646. <https://doi.org/10.1360/03wd0001>
- [10] Wang, S.Y., Zhang, L.X., Tao, P., Dai, C.G., Kuan, S.D., Wang, M. (2006). Geological characteristics and mineralization of Quartz-vein-type gold deposits in east of Guizhou. *Guizhou Geology*, 23(1): 36-43. <https://doi.org/10.3969/j.issn.1000-5943.2006.01.008>
- [11] Yang, R.D., Zhang, X.D., Liu, L., Yuan, S.T., Xu, L.Q. (2009). Geochemical characteristics of REE and trace element: Implication for gold source in the Xiajiang group of neoproterozoic Qingbaikouan system, Jinping County, Guizhou Province, China. *Acta Geologica Sinica*, 83(4): 505-514. <https://doi.org/10.3321/j.issn:0001-5717.2009.04.006>
- [12] Gu, L. (2000). Water-rock reaction experiment and discussion on metallogenic process of Mobin gold deposit and metallogenic mechanism of Southwest Hunan gold deposit. Doctoral thesis, Central South University, Changsha, China.
- [13] Gu, X.X., Zhang, Y.M., Schulz, O., Vavtar, F., Liu, J.M., Zheng, M.H., Zheng, L. (2012). The Woxi W-Sb-Au deposit in Hunan, South China: An example of late Proterozoic sedimentary exhalative (SEDEX) mineralization. *Journal of Asian Earth Sciences*, 57: 54-75. <https://doi.org/10.1016/j.jseaes.2012.06.006>
- [14] Zhu, Y.N., Peng, J.T., Liu, S.Y., Sun, Y.Z. (2014). Mineral deposit geology and trace element geochemistry of wolframite from the Woxi deposit, western Hunan, China. *Geochimica*, 87:104-112. <https://doi.org/10.1074/mcp.M113.034942>
- [15] Zeng, G.P., Gong, Y.J., Hu, X.L., Xiong, S.F. (2017). Geology, fluid inclusions, and geochemistry of the Zhazixi Sb-W deposit, Hunan, South China. *Ore Geology Reviews*, 91: 1025-1039. <https://doi.org/10.1016/j.oregeorev.2017.08.001>
- [16] Liu, A.L. (2018). Metallogenic regularity and prediction of gold deposits in southeast Guizhou. Doctoral thesis, China University of Geosciences, Wuhan, China.
- [17] Hodkiewicz, P.F., Groves, D.I., Davidson, G.J., Weinberg, R.F., Hagemann, S.G. (2009). Influence of structural setting on sulphur isotopes in Archean orogenic gold deposits, Eastern Goldfields Province, Yilgarn, Western Australia. *Mineralium Deposita*, 44: 129-150. <https://doi.org/10.1007/s00126-008-0211-5>
- [18] Zhang, Y.X. (1996). Gold deposits in China: Progress and reflections. Geological Publishing House, Beijing, China.
- [19] Zeng, G.P., Gong, Y.J., Hu, X.L., Xiong, S.F. (2017). Geology, fluid inclusions, and geochemistry of the Zhazixi Sb-W deposit, Hunan, South China. *Ore Geology Reviews*, 91: 1025-1039. <https://doi.org/10.1016/j.oregeorev.2017.08.001>
- [20] Zhang, T., Chen, Z., Huang, H., et al. (2020). Geochemical characteristics of gold-bearing minerals and its geological significance in the Ashaway gold deposit in the southwestern Tianshan Orogen. *Journal of Geomechanics*, 26(3): 443-458. <https://doi.org/10.12090/j.issn.1006-6616.2020.26.03.038>
- [21] Goldfarb, R.J., Ayuso, R., Miller, M.L., Ebert, S.W., Marsh, E.E., Petsel, S.A., Miller, L.D., Bradley, D., Johnson, C., McClelland, W., 2004, The late cretaceous Donlin Creek gold deposit, Southwestern Alaska: Controls on epizonal ore formation. *Economic Geology*, 99, 643-671. <https://doi.org/10.2113/99.4.643>
- [22] Korolev, N.M., Nikitina, L.P., Kuznetsov, A.B., Goncharov, A.G., Galankina, O.L., Shilovskikh, V.V., Vlasenko, N.S. (2023). Metasomatic origin of lamellar-like inclusions in clinopyroxenes from mantle xenoliths of the obnazhennaya pipe (Kuoika field, Yakutian Diamondiferous province). *Doklady Earth Sciences*, 510(2): 422-427.

- <https://doi.org/10.1134/S1028334X23600445>
- [23] Diamond, L.W. (2011). Review of the systematics of CO₂-H₂O fluid inclusions. *Lithos*, 55(1-4): 69-99. [https://doi.org/10.1016/S0024-4937\(00\)00039-6](https://doi.org/10.1016/S0024-4937(00)00039-6)
- [24] Mavrogenes, J.A., Henley, R.W., Tanner, D. (2011). Fluid inclusions in high sulphidation gold deposits: What can we learn from them about conditions of ore deposition? *European Current Research on Fluid Inclusions (ECROFI-XXI)*, Montanuniversität Leoben, Austria, pp. 142-143.
- [25] Liang, Y.H., Sun, X.M., Xu, L., Zhai, W., Liang, J.L., Tang, Q., Li, A.J. (2007). Fluids inclusions in quartz veins in HP-UHP metamorphic rocks from Chinese continental scientific drilling project. *Acta Petrologica Sinica*, 23(12): 3280-3286. <https://doi.org/10.3969/j.issn.1000-0569.2007.12.021>